Fundus Image Classification: A Wavelet Feature Descriptor Approach

Justice Kwame Appati
Department of Computer Science
University of Ghana
Accra, Ghana
jkappati@ug.edu.gh

Beatrice Armah
Department of Computer Science
University of Ghana
Accra, Ghana
btarmah@gmail.com

Ebenezer Owusu
Department of Computer Science
University of Ghana
Accra, Ghana
ebeowusu@ug.edu.gh

Michael Agbo Tettey Soli
Department of Computer Science
University of Ghana
Accra, Ghana
msoli@ug.edu.gh

2022 International Conference on Advancements in Smart, Secure and Intelligent Computing (ASSIC) | 978-1-6654-6109-2/22/$31.00 ©2022 IEEE | DOI: 10.1109/ASSIC55218.2022.10088415

***Abstract*—Lately, many diabetic patients are experiencing diabetic retinopathy resulting in a loss of their sight. Even though the urgency and threat posed by this condition, there is insufficient data source to engage appropriate computational intelligence tools. The few that exist happen to be imbalanced. Leveraging on this imbalanced dataset, several activities have been carried out to propose improved detection and classification descriptors. Although some works have been done in this domain, the issue of accuracy still persists in the administration of an effective diagnosis. This paper harnessed the benefits of Gabor filters and the multi-resolution property of Discrete Wavelet Transforms (DWTs) to construct appropriate fundus feature descriptors. These discriminant features are fed into some selected but predominant classical machine learning classifiers. Numerical evaluation of the study gave a perfect (100%) average score for the fundus image classification using Gradient Boosting and Logistic Regression classifiers over Accuracy, F1-score, Precision and Recall evaluation metric. The tie in performance is further broken using their computation time, suggesting that Logistic Regression is more appropriate with 9min 32sec over Gradient Boosting or 1hr 10min 32sec.**

Keywords—Diabetic Retinopathy, Discrete Wavelet Transform, Gabor feature extraction, Gradient Boosting, Logistic Regression

I. INTRODUCTION

Digital image processing techniques play a vital role in the area of medical imaging [4]. In this field of study, ophthalmologists depend heavily on the output of these images, especially in the screening and diagnosis of medical conditions such as macular edema, glaucoma, and Diabetic Retinopathy (DR). DR is a disease resulting from high blood vessels going through a series of deformities that eventually can lead to blindness [5-7]. It is a significant impediment to diabetes and a world-leading cause of the visual disorder when not detected early [8-9]. Regardless of age, symptoms of this condition are usually associated with floaters, blurred vision, flashes, and sudden loss of vision [10-11]. Conventionally, screening is conducted by an ophthalmologist, which requires extensive human capital [12], followed by a time-consuming [3] process in the weighing of several features for the classification of DR. One of these prominent early features of DR is microaneurysms, haemorrhages, and exudates [13]. The exudates are yellow-white spots with relatively well-defined margins formed due to the deposition of proteins and lipids leaked from damaged blood vessels of the retina. On the other hand, microaneurysms are central enlargement of retinal vessels which shows up as little round, dim red specks, while haemorrhages develop when blood spills from the retinal vessels [14]. In a few decades, computer vision for texture analysis and pattern recognition has found a suitable place in this domain for prominent feature extraction necessary for DR detection [15].

In the study of [2], the normality level in the retina fundus image using the classical Naïve Bayes classifier with 10-fold cross-validation was assessed. In evaluating the classifier, a dataset from the Eye Clinic of the Sakarya University Educational and Research Hospital was used. Their results showed up to 89% in accuracy and precision respectively. Again the study of [1] showed that changing the colour scheme of the fundus image from RGB to Lab shading space has a significant influence on performance. The radiance layer is first supplanted with the prepared data and converted back to the RGB shading space afterwards. The difference in the colour space is further improved using CLAHE with highlights such as shading, size, shape, edge quality and surface fed into a three-layer feed-forward neural network for exudates classification. Using the DIARETDB1 dataset, their model was assessed against mean sensitivity of 96.3% and precision of 93.7%.

Despite the extensive work done in this domain by the research community, studies are ongoing to define a more appropriate descriptor to characterize fundus image, which improves the overall performance of classical machine learning algorithms. In this study, it is observed that relying on the multi-resolution capability of the discrete wavelet transform coupled with Gabor filters for feature extraction, the Gradient Boasting and Logistic Regression classifier can achieve a perfect classification score of 100%. The rest of the paper is organized as follows: Section II discusses the source of data, the research design, the pre-processing tools and classifiers implemented in the study. Section III presents and discusses the results of the feature descriptor and the numerical evaluation of the models. The last section finally presents some recommendations and directions for future developments.

II. MATERIALS AND METHODS

A. Source of Data

In this study, a publicly available dataset, DIARETDB1 was used for the various experiments listed in Section III, with each image having a resolution of *1500 x 1152* in png format. The dataset contains 89 colored fundus images; out of which

978-1-6654-8695-8/22/$31.00 ©2022 IEEE

84 of them had non-proliferative signs of diabetic retinopathy, while the remaining 5 fundus images are without the signs of DR. Due to the imbalanced nature of the dataset as observed, image augmentation technique was employed to synthetically increase the number of good images to be at par with the DR infested images. In effect, the 5 retina fundus images were increased to 80 images signifying an additional 75 synthetic fundus images added to the original dataset. As a result, 164 retina fundus images were used to train and test the classifiers.

B. Research Design

Figure 1 is the research design implemented in this study. From the figure, the fundus image is preprocessed in the data wrangling phase, with its output fed into the feature extractor compartment. The resultant descriptor is trained with standard classification models and tested on the test dataset. Each classifier is then evaluated using accuracy, recall, precision, and f1-score.

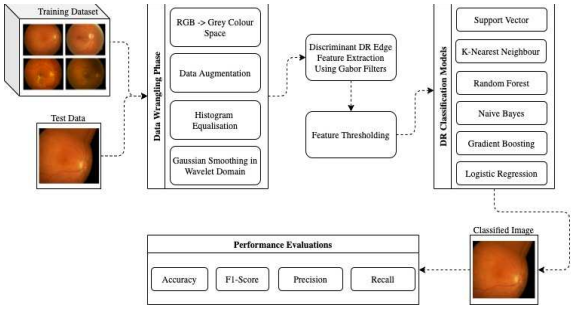

FIGURE 1: DESIGN PIPELINE

C. Data Wrangling Phase

The dataset in its natural state comes in a format not suitable for immediate use. This usually requires some prior activities, as detailed in the following subsections.

1) Data Preprocessing: The raw fundus image usually comes with radiance variety, contrast interestingly and clamour. These artefacts have a significant effect on the performance of classifiers when not dealt with appropriately in advance. In this study, issues of contrast in the image data are resolved with the adaptive histogram equalization (AHE). Before then, the present colour space of the image, which is RGB was changed to grey colour space

2) Data Augmentation: The current dataset used for this study happened to be unbalanced hence the need for other appropriate techniques to make the data balance. It was observed that the dataset was more skewed to the non-DR class. Even though the dataset was uneven, we proceeded to use it to test the performance of the feature descriptor. Ideally, it is expected to have the data balance in practice, so the classifier does not suffer memory loss. To address this, the data augmentation technique was used. This study used horizontal flip, rotation, zoom and width shift operators.

3) Discrete Wavelet Transform (DWT): The wavelet transform has enormous usage in several application domains, especially for data compression and noise removal. Depending on the type of representation of the data representation, thus either 1D or 2D, we have various kinds of wavelets defined for them. Among such types are Coiflets, Biorthogonal, Haar, Daubechies, Morlet, and Mexican Hat Symlets [23]. In this study, a 2D Haar wavelet was used for the noise removal task as they are relatively fast and simple to implement aside it being efficient. In its implementation, the image data is decomposed into four main subbands identified as LL, LH, HL, and HH. The LL denotes the coarser coefficient, and the three other subbands represent the finest scale wavelet coefficients [16]. Analogous to image edge analysis in the frequency domain, the HH subband denotes the diagonal edge details, with HL being the horizontal edge map while LH is the vertical edge map. On the other hand, the LL is the low-resolution estimate of the original image data. Since edge and noise are both characterised by high frequencies, it is expected that the HH subband will have a significant amount of noise embedded there, requiring some smoothing technique. Given the assumption that the predominant noise in medical images is Gaussian distributed, the gaussian noise filters are adopted to smoothen the high subbands. The LL subband can further be decomposed to obtain another level of decomposition until the desired number of levels determined by the application is reached. Mathematically, let $X_\phi(j,m,n)$ denote the approximation component (LL) and $X_\psi^H(j,m,n)$, $X_\psi^V(j,m,n)$, $X_\psi^D(j,m,n)$ denotes the three detail coefficients (LH, HL, HH) respectively. With this notation, the DWT computation of the 2D data x (Eqn. 1) and its inverse (Eqn. 2) is defined as

$$X = HxH^T \tag{1}$$

$$x = H^T XH \tag{2}$$

where H is the appropriate 1D haar transform matrix. With the single-scale N-point 1D transform matrix, H is partitioned as

$$H = \begin{bmatrix} [L] \\ [H] \end{bmatrix} \tag{3}$$

Substitution Eqn. 3 into Eqn. 1 we have Eqn. 4

$$X = \begin{bmatrix} L \\ H \end{bmatrix} x \begin{bmatrix} L \\ H \end{bmatrix}^T = \begin{bmatrix} Lx \\ Hx \end{bmatrix} [L^T \quad H^T]$$

$$X = \begin{bmatrix} LxL^T & LxH^T \\ HxL^T & HxH^T \end{bmatrix} = \begin{bmatrix} X_\phi & X_\psi^H \\ X_\psi^V & X_\psi^D \end{bmatrix} \tag{4}$$

Conversely, x can be reconstructed from Eqn. 4 using Eqn. 2.

4) Feature Extraction with Gabor Filters: The Gabor filter is an implementation of the Gabor transform, which is a short term Fourier transformation with a Gaussian window for spatial domain analysis. It has gained significant recognition in many application domains in a few decades due to its optimal localization properties in both spatial and frequency domains. It has been used successfully as a feature descriptor for fingerprint recognition [18], edge detection [19], face recognition [20], texture segmentation / classification [21], character recognition [22] and image compression. Gabor is used for edge detection after obtaining the wavelet denoised image in this study. In its implementation [17], the Gabor filters are convolved with the image intensity *I(x,y)* at every pixel *(x,y)* as Eqn. 5.

$$G(x,y;f_k,\theta_m)=\sum_{x'}\sum_{y'}I(x-x',y-y')h(x',y';f_k,\theta_m) \quad (5)$$

The 2D Gabor function h, from Eqn. e1 in its general function form in terms of the spatial domain impulse response, and its frequency domain response is defined as Eqn. 6.

$$h(x,y;f,\theta)=\frac{1}{\sqrt{\pi\sigma_1\sigma_2}}\exp\left(-\frac{1}{2}\left(\frac{R_1^2}{\sigma_1^2}+\frac{R_2^2}{\sigma_2^2}\right)\right)\cdot\exp\left(i\left(f_x x+f_y y\right)\right) \quad (6)$$

where $R_1=xcos\theta+ysin\theta$; $R_2=-xsin\theta+ycos\theta$; $\sigma_1=\frac{c_1}{f}$; $\sigma_2=\frac{c_2}{f}$; $f_x=fcos\theta$; $f_y=fsin\theta$; c_1 and c_2 are two constants. The parameters, σ_1 and σ_2 are the standard deviations of the 2D Gaussian function, f is the central frequency, and θ is the spatial orientation. From Eqn. 5, The phase information of $G(f_k,\theta_m)$ can be taken as features as it contains information about the edge location and other details in the image. On the other hand, the amplitude can also be taken as features as it contains some orientated frequency spectrum in every local of the image *I*. Figure 2 is a sample image of the fundus image after applying the discrete Gabor filters.

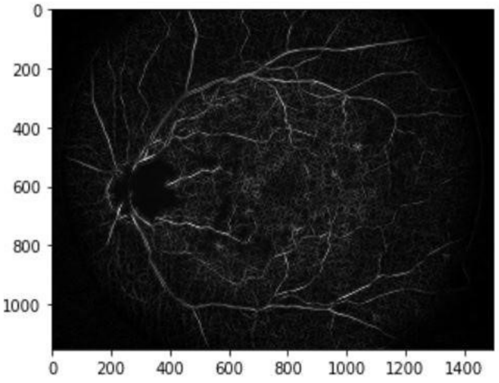

FIGURE 2: SAMPLE GABOR FILTERED IMAGE

D. DR Classification Techniques

This section gives, in brief, a description of some selected learning algorithms used in this study to classify the DR fundus images.

1) Support Vector Machine: Support vector machine (SVM) is one of the widely used machine learning techniques for prediction and classification analysis [26]. This technique was derived from statistical learning theory by Vapnik et al. in 1992, and it is widely used because it chooses a classification hypothesis in such a way to maximize its generalization ability between two disjoint half-spaces [25]. In instances where the data points are not linearly separable in the input space, a nonlinear transformation function known as the kernel is required to transform the data to a higher-dimensional space. To a large extent, the performance of SVM depends significantly on the a priori choice of these kernel functions. Classically examples of these kernels are: linear, multilayer perceptron, polynomial and Gaussian [24]. Mathematically, let $\{S=\{(x^i,y^i),x^i\in\Re^n,y^i\in\{-1,1\},i\in I,card(I)=N\}$ be a linearly separable training set, then the hyperplane w that solves the optimization problem $\min_{w,b}<w\cdot w>$ subject to the constraints, $y^i(<w\cdot x^i>+b)\geq 1;\ i=1,2,\cdots,N$ realizes the maximum margin hyperplane with geometric margin $\gamma=\frac{1}{||w||_2}$. The solution to this problem is obtained by solving the dual in Eqn. 7

$$\max\sum_{i=1}^{N}\alpha_i-\frac{1}{2}\sum_{i=1}^{N}\sum_{j=1}^{N}y^iy^j\alpha^i\alpha^j<x^i\cdot x^j> \quad (7)$$

subject to the constraints in Eqn. 8

$$\sum_{i=1}^{N}y^i\alpha^i=0 \quad (8)$$
$$\alpha^i\geq 0,\quad i=1,2,\cdots,N$$

If the parameters, a^* and b^* are the solution to the optimization problem, the required optimal hyperplane can be expressed in the dual representation as Eqn. 9.

$$f(x,a^*,b^*)=\sum_{i=1}^{N}y^ia^{i^*}<x^i.x>+b^* \quad (9)$$

2) Logistic Regression: The logistic regression model is also a well-known and fundamental technique for classification. Several variants of this technique exist; however, the most common form that results in a binary outcome is used based on the dataset's structure. In logistic regression [27], the conditional probability of the output class say y, is modelled as a logit-transformed multiple linear regression of the input features say $[x_1|x_2|\cdots|x_n]$ as expressed in Eqn. 10.

$$\mathrm{P}(\mathrm{y}=\pm 1|\mathrm{x},\mathrm{w})=\frac{1}{1+\mathrm{e}^{-\mathrm{y}\mathrm{w}^{\mathrm{T}}\mathrm{x}}} \quad (10)$$

The parameter w in this equation is estimated by maximizing the likelihood of the equation on the given fundus training dataset using Eqn. 11.

$$\prod_{\mathrm{i}=1}^{2}\mathrm{P}(\mathrm{y}_\mathrm{i}|\mathrm{x}_\mathrm{i},\mathrm{w})=\prod_{\mathrm{i}=1}^{2}\frac{1}{1+\mathrm{e}^{-\mathrm{y}_\mathrm{i}\mathrm{w}^{\mathrm{T}}\mathrm{x}_\mathrm{i}}} \quad (11)$$

By penalizing the complexity of Eqn. 11 using Eqn. 12, the maximization problem can be restated as the minimization of the regularized negative log-likelihood in Eq. 13.

$$\frac{1}{\sigma\sqrt{2\pi}}\mathrm{e}^{-\frac{1}{2\sigma^2}\mathrm{w}^{\mathrm{T}}\mathrm{w}} \quad (12)$$

$$\rho=\mathrm{C}\sum_{\mathrm{i}=1}^{2}\log\left(1+\mathrm{e}^{-\mathrm{y}_\mathrm{i}\mathrm{w}^{\mathrm{T}}\mathrm{x}_\mathrm{i}}\right)+\mathrm{w}^{\mathrm{T}}\mathrm{w} \quad (13)$$

Eqn. 13 can be solved using the coordinate descent approach described in [28].

E. Performance Evaluation

This study used the recall (RC), precision (PR), F1 score (F_1C) and accuracy (AC) for the performance evaluation of the models discussed in Section 2.5. These metrics are computed using four standard variables thus: false negative (FN), true negative (TN), false positive (FP), and true positive (TP). The closer the metrics are to the value one (1), the better the performance of the selected model [30]. The recall metric is a measure of the likelihood that a randomly selected important instance will be predicted as positive as expressed mathematically in Eqn. 14. On the other hand, the accuracy metric is the measure of the likelihood that a randomly chosen instance, either positive or negative, relevant or irrelevant, will be predicted correctly as expressed mathematically in

Eqn. 15. The other two ratios (PR and F_1C) are stated algebraically in Eqn. 16 and Eqn. 17 respectively [29].

$$RC = \frac{TP}{TP + TN} \tag{14}$$

$$AC = \frac{TP + FN}{TP + FP + TN + FN} \tag{15}$$

$$PR = \frac{TP}{TP + FP} \tag{16}$$

$$F_1C = \frac{2 * PR * RC}{PR + RC} \tag{17}$$

III. Results and Discussion

This section discusses the results of the various methods used. It shows the classification models' performance and compares the results against accuracy, precision, recall, and f1-score. All the six classification models were used to detect diabetic retinopathy, and among the six, two of them gave a better performance. The models were trained and tested using Python 3.7 language (Anaconda) with Jupyter Notebook 6.0.3 running on a PC computer 4quipped with Intel i5-8265U CPU @ 1.60GHz 1.80GHz processor. Subsequent sections gives details of the results.

A. Augmented Image Analysis and Findings

1) Support Vector Machine: This section discusses the findings using only the Support Vector Machine. The model's performance is analyzed using the output of the confusion matrix.

a) SVM – Linear: The observation recorded an accuracy of 52%, F1-score 68%, precision of 51%, and recall of 100% after training. The confusion matrix predicted (2 images) as true positive (78 images) as false positive, (0) as false-negative, and (84 images) as true negative. The test time was 12 minutes, 20 seconds. With the SVM's performance – Linear shown above, Accuracy shows 52% and F1-score 68%. The confusion matrix in Table 1 shows that 2 of the images were classified as true positives, while 78 images were classified as false positives. Meanwhile, 80 images are classified as true positives, which indicates that the model could not predict the image correctly. In this case, F1-score is high only when both Recall and Precision are high. Nevertheless, the F1 Score is considered a better measure than Accuracy because the F1 score relay on Precision and Recall. Only Precision can not be considered a useful measure in the confusion matrix, neither Recall nor Accuracy. However, since the F1 Score combines both Precision and Recall, it gives a better result. This shows that utilizing a confusion matrix to evaluate a model's performance gives a fair idea of whether the model is good for the training. Per the analysis, Accuracy can result in the misleading interpretation of results when considered a sole measure for performance.

TABLE 1. CONFUSION MATRIX FOR SVM – LINEAR

		ACTUAL	
		Positive	Negative
PREDICTED	Positive	2	78
	Negative	0	84

b) SVM – Radial Basis Function (RBF): The observation recorded an accuracy of 51%, F1-score 67%, precision of 51%, and recall of 100% after training. The confusion matrix predicted (0) true positive, (80 images) as false positive, (0) as false-negative, and (84 images) as true negative. The test time was 14 minutes 16 seconds. Table 2 shows that none of the images was classified as true positives, and 84 images are classified as true negatives; the F1-score was 67% because both Precision and Recall have a high result. Accuracy is also 51% but can not be used because it can mislead the results' interpretation. In this case, the confusion matrix has influenced the model's performance, which shows that 80 images were not classified correctly as true positive. The same observation recorded in Table 2 was noted for both sigmoid & polynomial functions.

TABLE 2. CONFUSION MATRIX FOR SVM - RBF

		ACTUAL	
		Positive	Negative
PREDICTED	Positive	0	80
	Negative	0	84

2) K-Nearest Neighbor: This section discusses the findings using only K-nearest neighbours. The model's performance is analyzed using the output of the confusion matrix.

TABLE 3. CONFUSION MATRIX FOR K-NEAREST NEIGHBOUR

		ACTUAL	
		Positive	Negative
PREDICTED	Positive	76	4
	Negative	9	75

The observation after training recorded an accuracy of 93%, F1-score 93%, precision 95%, and recall of 91% where the confusion matrix predicted (76 images) as true positive, (4 images) as false positive, (9) as false-negative, and (75 images) as true negative. The test time was 12 minutes, 6 seconds. Table 3 shows that 76 images were classified correctly as true positives and 75 images as true negatives; the F1-score was 93% because both Precision and Recall have a high result. Accuracy is also 93% but can not be used because it can mislead interpretation of the results. The confusion matrix has influenced the model's performance, which shows that four images were not classified correctly as true positive, and seven images were also not classified as false negatives.

3) Random Forest: This section discusses the findings using only the Random Forest. The model's performance is analyzed using the output of the confusion matrix.

TABLE 4. CONFUSION MATRIX FOR RANDOM FOREST

		ACTUAL	
		Positive	Negative
PREDICTED	Positive	1	79
	Negative	0	84

The observation after training recorded an accuracy of 95%, F1-score 97%, precision 96%, and recall 98% where the confusion matrix predicted (1 image) as true positive, (79 images) as false positive, (0) as false-negative, and (84 images) as true negative. The test time was 12 minutes 7 seconds. Table 4 shows that only one image was classified correctly as true positives, and 84 images are classified as true negatives; the F1-score was 68% because both Precision and Recall have a high result. Accuracy is also 51% but can not be used because it can mislead the results' interpretation. In this case, the confusion matrix has influenced the model's

performance, which shows that 79 images were not classified correctly as true positives.

4) Naïve Bayes: This section discusses the findings using only Naïve Bayes Theorem. The model's performance is analyzed using the output of the confusion matrix.

TABLE 5. CONFUSION MATRIX FOR NAÏVE BAYES THEOREM

		ACTUAL	
		Positive	Negative
PREDICTED	Positive	50	30
	Negative	31	53

The observation recorded an accuracy of 62%, F1-score 63%, precision of 63%, and recall 63% after training. The confusion matrix predicted (50 images) as true positive, (30 images) as false positive, (31 images) as false negative, and (53 images) as true negative. The test time was 12 minutes 10 seconds. Table 5 shows that 50 images were classified correctly as true positives, and 53 images were classified correctly as true negatives; the F1-score was 63% because both Precision and Recall have a high result. Accuracy is 62% but can not be used because it can mislead the interpretation of the results. In this case, the confusion matrix has influenced the model's performance, which shows that 30 images were not classified correctly as true positives, and 31 images were not classified correctly as true negatives.

5) Gradient Boosting: This section discusses the findings using only Gradient Boosting. The model's performance is analyzed using the output of the confusion matrix.

TABLE 6. CONFUSION MATRIX FOR GRADIENT BOOSTING

		ACTUAL	
		Positive	Negative
PREDICTED	Positive	80	0
	Negative	0	84

The observation recorded 100% accuracy, F1-score 100%, Precision 100%, and recall 100% after training. The confusion matrix predicted (80 images) as true positive, (0) as false positive, (0) false-negative, and (84 images) as true negative. The test time was 1hr 10 minutes 32 seconds. Table 6 shows that 80 images were classified correctly as true positives, and 84 were classified as true negatives, which makes the F1-score 100% because both Precision and Recall have a high result. Accuracy is also 100% but can not be used because it can mislead interpretation of the results. In this case, the confusion matrix has influenced the model's performance, giving it better and good results. The confusion matrix helps indicate whether the model was classified correctly or not.

6) Logistic Regression: This section discusses the findings using only Logistic Regression. The model's performance is analyzed using the output of the confusion matrix.

TABLE 7: CONFUSION MATRIX FOR LOGISTIC REGRESSION

		ACTUAL	
		Positive	Negative
PREDICTED	Positive	80	0
	Negative	0	84

The observation recorded 100% accuracy, F1-score 100%, Precision 100%, and recall 100% after training. The confusion matrix predicted (80 images) as true positive, (0) as false positive, (0) false-negative, and (84 images) as true negative. The test time was 9minutes 15seconds.

Table 7 shows that 80 images were classified correctly as true positives and 84 as true negatives, making the F1-score 100% because both Precision and Recall have a high result. Accuracy is also 100% but can not be used because it can mislead interpretation of the results. In this case, the confusion matrix has influenced the model's performance, giving it better and good results.

B. Comparative Analysis

The methods have been tested by extracting the required features from the retinal fundus images: the exudates' diameter, microaneurysms, and haemorrhages. However, the classification is applied to identify the class label and evaluate the experimental results. The performance of the trained models is evaluated. Along these lines, prescient Accuracy has been utilized as a presentation measure for picture characterization. The forecast exactness is estimated as a proportion of effectively characterized occasions in the test dataset and the all outnumber experiments. The six classifiers' exhibitions are evaluated based on three criteria: Precision, F1-score, and Recall. Accuracy is also a criterion to measure the overall performance of the classification. The comparative results of the various classifiers are shown in Table 8.

TABLE 8. COMPARATIVE RESULTS OF VARIOUS CLASSIFIERS

Models	Accuracy	F1-score	Precision	Recall
SVM	0.52	0.68	0.51	1.0
KNN	0.93	0.93	0.95	0.91
NBT	0.61	0.58	0.65	0.53
GB	1.0	1.0	1.0	1.0
LR	1.0	1.0	1.0	1.0
RF	0.51	0.68	0.51	1.0

C. Discussion

The analysis in Table 8 shows that the Gradient Boosting classifier and Logistic Regression classifier give a higher prediction presentation of the model. Even though SVM is one of the best classification models for binary classification problems and multi-classification, its performance compared to other classifiers was not better than Gradient Boosting and Logistic Regression. Furthermore, the true negative was predicted correctly, but the true positive was not predicted as required but rather was seen as a false positive; due to this result, SVM can not give good judgment on a healthy eye in detecting or predicting familiar fundus image. In this regard, Gradient Boosting and Logistic Regression gave good judgment on the healthy eye and abnormal eye. As a result, these two classification methods are reliable for detecting and predicting diabetic retinopathy patients with accurate and timely results. In the performance measure, both classifiers gave 100% Precision, Recall, F1-score, and Accuracy, respectively. Compared with the other classifiers, their performance is higher and better at all angles. Even though both classifiers performed well, the output time is different, which means that one response time is faster than the other, and that makes that one best chosen for future research like this one. The response time for Logistic Regression is faster than Gradient Boosting. Gradient Boosting's test time was 1hr 10 minutes 32 seconds, while Logistic Regression test time was 9 minutes 32 seconds. This makes it clear which classifier is best for quick response time.

IV. Conclusions and Recommendation

In this study, a grouping that utilizes measurable highlights got from the blend of the discrete wavelet change and Gabor channel to characterize typical pictures versus malignant growth pictures, utilizing Gradient Boosting and Logistic Regression classifiers. Although SVM is a perfect classification model, it could not predict the true positive of the dataset but could predict the true negative rightly. SVM's performance measure was Accuracy of 51%, F1-score 68%, Precision 51%, and recall 100%. While the performance measure of Gradient boosting and Logistic regression was 100% for Accuracy, Precision, F1-score, and Recall. The results show that such a crossover handling model accomplishes higher Precision than utilizing DWT or Gabor channel banks alone. Based on the experiments, the system can detect abnormalities accompanied by diabetic retinopathy. The signs of diabetic retinopathy, exudates, microaneurysms, and haemorrhages are challenging to detect because of other typical retinal characteristics with comparative features like contrast, power levels, shape, and colour. However, it has been shown that Discrete wavelet transform and Gabor filter statistical features offer an efficient solution for these issues. Early discovery and finding of Diabetic Retinopathy help the patients from vision misfortune, and the seriousness of the malady can be decreased.

References

[1] Franklin, S. W., & Rajan, S. E. (2014). Diagnosis of diabetic retinopathy by employing image processing technique to detect exudates in retinal images. *Image Processing, IET, 8*, 601-609.

[2] Sudha, V., & Karthikeyan, C. (2018). Analysis of diabetic Retinopathy using naive bayes classifier technique. *International Journal of Engineering & Technology, 7*(2.21), 440-442.

[3] Kwasigroch, A., Jarzembinski, B., & Grochowski, M. (2018). Deep CNN based decision support system for detection and assessing the stage of diabetic retinopathy. *2018 International Interdisciplinary PhD Workshop (IIPhDW)* (pp. 111-116). IEEE.

[4] Lachure, J., Deorankar, A. V., Lachure, S., Gupta, S., & Jadhav, R. (2015). Diabetic retinopathy using morphological operations and machine learning. *2015 IEEE International Advance Computing Conference (IACC)* (pp. 617-622). IEEE.

[5] El Sisy, A. S., Salem, N. M., & Seddik, A. F. (2015). Automatic Detection of Exudates from Digital Color Fundus Images. *International Journal of Computer Applications, 122*(7), 18-22.

[6] Lin, G. M., Chen, M. J., Yeh, C. H., Lin, Y. Y., Kuo, H. Y., Lin, M. H., . . . Cheung, C. Y. (2018). Transforming retinal photographs to entropy images in deep learning to improve automated detection for diabetic retinopathy. *Journal of Ophthalmology, 2018, ArticleID: 2159702*.

[7] Umapathy, A., Sreenivasan, A., Nairy, D. S., Natarajan, S., & Rao, B. (2019). Image Processing, Textural Feature Extraction and Transfer Learning-based detection of Diabetic Retinopathy. *Proceedings of the 2019 9th International Conference on Bioscience, Biochemistry and Bioinformatics* (pp. 17-21). ACM.

[8] Bhattacharya, S., Sehgal, J., Issac, A., Dutta, M. K., Burget, R., & Kolarik, M. (2018). Computer vision method for grading of health of a fundus image on basis of presence of red lesions. *2018 41st International Conference on Telecommunications and Signal Processing (TSP)* (pp. 1-6). IEEE.

[9] Sopharak, A., Uyyanonvara, B., Barman, S., & Williamson, T. H. (2008). Automatic detection of diabetic retinopathy exudates from non-dilated retinal images using mathematical morphology methods. *Computerized Medical Imaging and Graphics, 32*, 720-727.

[10] Santhakumar, R., Tandur, M., Rajkumar, E. R., Geetha, K. S., Haritz, G., & Rajamani, K. T. (2016). Machine learning algorithm for retinal image analysis. *2016 IEEE Region 10 Conference (TENCON)* (pp. 1236-1240). IEEE.

[11] Salamat, N., Missen, M. M., & Rashid, A. (2019). Diabetic retinopathy techniques in retinal images: a review. *Artificial intelligence in medicine, 97*, 168-188.

[12] Jiang, Y., Wu, H., & Dong, J. (2017). Automatic screening of diabetic retinopathy images with convolution neural network based on Caffe framework. *1st International Conference on Medical and Health Informatics 2017* (pp. 90-94). ACM.

[13] Pratt, H., Coenen, F., Broadbent, D. M., Harding, S. P., & Zheng, Y. (2016). Convolutional neural networks for diabetic retinopathy. *Procedia Computer Science, 90*, 200-205.

[14] Kazakh-British, N. S., Pak, A. A., & Abdullina, D. (2018). Automatic Detection of Blood Vessels and Classification in Retinal Images for Diabetic Retinopathy Diagnosis with Application of Convolution Neural Network. *2018 International Conference on Sensors, Signal and Image Processing* (pp. 60-63). ACM.

[15] Murala, S., Maheshwari, R. P., & Balasubramanian, R. (2012). Local tetra patterns: a new feature descriptor for content-based image retrieval. *IEEE transactions on image processing, 21*(5), 2874-2886.

[16] Lai, C.-C., & Tsai, C.-C. (2010). Digital image watermarking using discrete wavelet transform and singular value decomposition. *IEEE Transactions on Instrumentation and Measurement, 59*(11), 3060–3063.

[17] Zheng, D., Zhao, Y., & Wang, J. (2004). FEATURES EXTRACTION USING A GABOR FILTER FAMILY. *6th IASTED International Conference* (pp. 139-144). Honolulu, Hawaii, USA: Signal and Image Processing.

[18] Yang, J., Liu, L., Jiang, T., & Fan, Y. (2003). A modified Gabor filter design method for fingerprint image enhancement. *Pattern Recognition Letters, 24*(12), 1805-1817.

[19] Namuduri, K., Mehrotra, R., & Ranganathan, N. (1992). Edge detection models based on Gabor filters. *11th IAPR International Conf. On Speech and Signal Analysis Proceedings* (pp. 729-732). IEEE .

[20] Liu, C., & Wechsler, H. (2003). Independent Component Analysis of Gabor Features for Face Recognition. *IEEE Trans. on Neural Networks, 14*(4), 919-928.

[21] Bodnarova, A., Bennamoun, M., & Latham, S. (2002). Optimal Gabor filters for textile flaw detection. *Pattern Recognition, 35*(12), 2973-2991.

[22] Yih-Ming, S., & Jhing-Fa, W. (2003). A novel stroke extraction method for Chinese characters using Gabor filters. *Pattern Recognition, 36*(3), 635-647.

[23] Amoako-Yirenkyi, P., Frempong, N., Appati, J., Hafron-Acquah, J., & Dontwi, I. (2015). Threshold analysis of wavelet based fingerprint feature extraction methods on multiple impression dataset. *Journal of Advances in Mathematics and Computer Science, 5*(3), 383-396.

[24] Appati, J. K., Gogovi, G. K., & Fosu, G. O. (2014). On the selection of appropriate kernel function for svm in face recognition. *International Journal of Advanced Research in Computer Science and Software Engineering, 4*(3), 6-9.

[25] Cristianini, N., & Shawe-Taylor, J. (2000). *An Introduction to Support Vector Machines and Other Kernel Based Learning Methods.* Cambridge, UK,: Cambridge University Press.

[26] Zhang, Y., Sun, X., Bajwa, S. G., Sivarajan, S., Nowatzki, J., & Khan, M. (2018). Plant Disease Monitoring With Vibrational Spectroscopy. *Comprehensive Analytical Chemistry, 80*, 227-251.

[27] Caie, P. D., Dimitriou, N., & Arandjelović, O. (2021). Precision medicine in digital pathology via image analysis and machine learning. *Artificial Intelligence and Deep Learning in Pathology*, 149-173.

[28] Yu, H.-F., Huang, F.-L., & Lin, C.-J. (2011). Dual coordinate descent methods for logistic regression and maximum entropy models. *Machine Learning, 85*(1-2), 41-75.

[29] Appati, J. K., Nartey, P. K., Owusu, E., & Denwar, I. W. (2021). Implementation of a Transform-Minutiae Fusion-Based Model for Fingerprint Recognition. *International Journal of Mathematics and Mathematical Sciences, 2021, ArticleID: 5545488*.

[30] Appati, J. K. (2021). Performance and Applicability of Transfer Learners for Cocoa Swollen Shoot Detection. *International Journal of Technology Diffusion, 12*(2), 68-77.